The Astrophysical Journal Letters, 813:L28 (6pp), 2015 November 10 doi:10.1088/2041-8205/813/2/L28

THE FRACTIONS OF INNER- AND OUTER-HALO STARS IN THE LOCAL VOLUME

Deokkeun An[1], Timothy C. Beers[2], Rafael M. Santucci[3], Daniela Carollo[2],
Vinicius M. Placco[2], Young Sun Lee[4], and Silvia Rossi[3]
[1] Department of Science Education, Ewha Womans University, 52 Ewhayeodae-gil, Seodaemun-gu, Seoul 03760, Korea; deokkeun@ewha.ac.kr
[2] Department of Physics and JINA Center for the Evolution of the Elements, University of Notre Dame, Notre Dame, IN 46556, USA
[3] Departamento de Astronomia, Instituto de Astronomia, Geofísica e Ciências Atmosféricas, Universidade de São Paulo, São Paulo, SP 05508-900, Brazil
[4] Department of Astronomy & Space Science, Chungnam National University, Daejeon 34134, Korea
Received 2015 August 17; accepted 2015 October 21; published 2015 November 3

ABSTRACT

We obtain a new determination of the metallicity distribution function (MDF) of stars within ∼5–10 kpc of the Sun, based on recently improved co-adds of *ugriz* photometry for Stripe 82 from the Sloan Digital Sky Survey. Our new estimate uses the methodology developed previously by An et al. to study in situ halo stars, but is based on a factor of two larger sample than available before, with much-improved photometric errors and zero-points. The newly obtained MDF can be divided into multiple populations of halo stars, with peak metallicities at [Fe/H] ≈ -1.4 and -1.9, which we associate with the inner-halo and outer-halo populations of the Milky Way, respectively. We find that the kinematics of these stars (based on proper-motion measurements at high Galactic latitude) supports the proposed dichotomy of the halo, as stars with retrograde motions in the rest frame of the Galaxy are generally more metal-poor than stars with prograde motions, consistent with previous claims. In addition, we generate mock catalogs of stars from a simulated Milk Way halo system, and demonstrate for the first time that the chemically and kinematically distinct properties of the inner- and outer-halo populations are qualitatively in agreement with our observations. The decomposition of the observed MDF and our comparison with the mock catalog results suggest that the outer-halo population contributes on the order of ∼35%–55% of halo stars in the local volume.

Key words: Galaxy: abundances – Galaxy: evolution – Galaxy: formation – Galaxy: halo – Galaxy: stellar content

1. INTRODUCTION

While many details of the galaxy-formation process remain largely unresolved, it is generally believed that large spiral galaxies like the Milky Way have been assembled from numerous low- to intermediate-mass clumps of stars and gas, each of which is found in its own dark matter sub-halos, through mergers and accretions onto more massive halos. The emerging picture, supported by a number of recent large cosmological simulations (e.g., Zolotov et al. 2009; Font et al. 2011; Tissera et al. 2012, 2013), is a generic expectation that the metallicity distribution functions (MDFs), kinematics, and spatial distributions of the stellar populations formed primarily from early mergers and in situ star formation differ from those that formed primarily from accretion.

In the past decade our view of the nature of the halo of the Galaxy has also evolved substantially, with considerable observational support for the suggestion that it comprises at least two distinct diffuse stellar components, the inner-halo and outer-halo populations (Carollo et al. 2007, 2010; de Jong et al. 2010; Nissen & Schuster 2010; Beers et al. 2012; Schuster et al. 2012; An et al. 2013, and references therein), with substantial contributions from the debris of relatively recent accretion events (such as the Sagittarius Stream) in the outer regions of the halo (Janesh et al. 2015), in contrast to the previously assumed monolithic halo. In any event, it is clear that full understanding of the complex nature of the Milky Way's halo system is required in order to constrain models for the structural and chemical evolution of large spirals like our own.

The first inferences for a dual halo relied on a sample of stars exploring only a nearby region ($d_{\rm Sun} \leqslant 4$ kpc), so that accurate proper motions could be used (Carollo et al. 2007, 2010). This led to criticism (e.g., Schönrich et al. 2011; refuted by Beers et al. 2012) that the derived space motions were affected by distance-scale errors, creating the illusion of a dual halo. Interpretations based on more distant in situ samples of stars, exploring regions many tens of kpc away (Allende Prieto et al. 2014; Chen et al. 2014; Fernandez-Alvar et al. 2015), have now firmly established the presence of trends in the mean metallicities, as well as in individual abundance ratios ([Ca/Fe], [Mg/Fe]), indicating that the diffuse halo outside the local region behaves in essentially the manner required by the initial claims of Carollo et al. and others. The apparent differences in the frequencies of the sub-classes of carbon-enhanced metal-poor stars (see Beers & Christlieb 2005) that can be associated with the inner- and outer-halo populations are also difficult to reconcile with a single-halo model (Carollo et al. 2012, 2014).

Another limiting factor in consideration of the nature of the halo is that it has proven extremely challenging to assemble what might be referred to as a "fair" sample of stellar probes. "Historical samples," going back to selections based on high proper motions (e.g., Ryan & Norris 1991) necessarily confounded kinematics with chemistry, under the assumption that this would not severely impact interpretations of the MDF from a single-halo population. Others approached the problem by selecting samples of halo stars based on the apparent weakness of metallic lines (in particular Ca II K) from objective-prism surveys, which necessarily distorts the MDF of the more metal-rich stars in favor of producing samples of the most metal-poor stars (Beers & Christlieb 2005; Frebel & Norris 2015).

An alternative approach to the above was first explored by Ivezić et al. (2008a), who produced a photometric-metallicity map based on estimates from SDSS *ugr* photometry, although

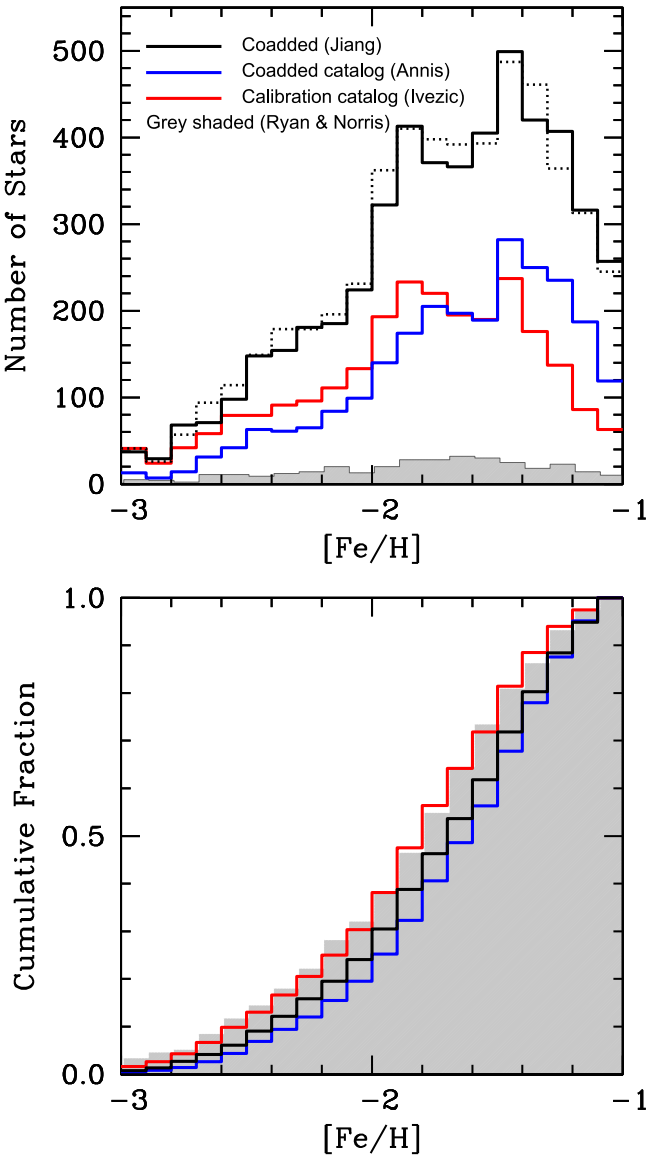

Figure 1. Top panel: comparison of the new MDF from the J14 (black solid line) co-add catalog with those derived in A13 using the calibration (Ivezić et al. 2007, red solid line) and co-add (Annis et al. 2014, blue solid line) catalogs. The gray region is the MDF from the spectroscopic sample of Ryan & Norris (1991). The black dotted line shows the MDF derived from the J14 catalog, but after applying photometric zero-point corrections found in Yuan et al. (2015b). Bottom panel: cumulative MDFs for the above samples. Note that, although there are more stars included in the newer catalog, the overall shapes of MDF are similar to one another.

it was acknowledged that the techniques employed failed for metallicities [Fe/H] < -2.0, so tests for the presence of a very low-metallicity outer-halo population could not be made.

An et al. (2013, hereafter A13) explored a refined approach to the photometric metallicity-estimation technique, based on comparisons of *ugriz* photometry with well-calibrated cluster fiducial sequences. For a sample of several thousand stars from SDSS Stripe 82, selected to span a limited range of main-sequence mass and apparent magnitude (resulting in distance limits 5–8 kpc from the Sun), A13 were able to obtain the first fair sample of local halo stars, one that is unbiased in *both* kinematics and chemistry (covering the metallicity range $-2.5 \leqslant$ [Fe/H] $\leqslant -1.0$, and perhaps a little lower). The relatively limited number of stars in their final sample ($N \sim 2500$) and the influence of photometric errors on metallicity estimates at the low end of the MDF prevented them from confirming the presence of a dual halo from the derived MDF alone, as compared to a "simple model" distribution (e.g., Hartwick 1976; Norris & Ryan 1991)—the data were statistically consistent with being drawn from either model of the parent population. However, A13 *were* able to demonstrate, on the basis of an approximate rotational measure (derived from proper motions of stars at high Galactic latitudes) that stars with retrograde velocities clearly favored the lowest metallicity stars in their sample, and concluded that a single halo population was inconsistent with this result.

Recently, Jiang et al. (2014, hereafter J14) revisited the SDSS Stripe 82 *ugriz* data, producing a "depth optimized" co-add sample with fainter limiting magnitudes and reduced errors in the final photometry. Yuan et al. (2015a) used these data to assemble a catalog of photometric metallicity estimates for a half million stars, spanning a large color and metallicity range. It appears, however, that their method of metallicity estimation suffers from similar limitations at low metallicity as did the Ivezić et al. (2008a) approach, rendering it unsuitable for exploration of the halo MDF for [Fe/H] $\lesssim -2.0$, where the potential contribution from outer-halo stars becomes dominant. Hence, in the present paper we have used the approach of A13 and apply it to the J14 co-adds, in order to explore anew the nature of the derived halo MDF with a substantially larger sample of stars with improved photometric metallicity estimates.

2. THE UPDATED SDSS CO-ADD PHOTOMETRY

We employed *ugriz* photometry for Stripe 82 from the co-added imaging frames in J14, a catalog that is almost two magnitudes deeper than the single-epoch photometry in SDSS. Compared to Annis et al. (2014), the photometry is also deeper by 0.3–0.5 mag, due to the use of more repeated image scans in the co-add procedure. Following the prescription in J14, we used aperture photometry with 8 pixel (3.″2) diameter aperture, and applied aperture corrections based on the difference from the photometry with 20 pixel (8.″0) aperture for relatively bright stars ($15 < r < 18$) in each field. We selected good photometry based on the `SExtractor` extraction flag set to zero in each band. We then assembled matched photometry in five filter passbands using a 1″ search radius.

3. SAMPLE SELECTION

Figure 12 of A13 illustrates our selection of halo main-sequence stars. Higher-mass main-sequence stars can be used to probe a more distant volume than lower-mass stars, because they are intrinsically brighter than less-massive ones. The mass–luminosity relations also depend strongly on metallicity, so metal-poor stars are seen at larger distances at a given stellar mass. These relatively well-known relations between stellar mass, luminosity, and metallicity set a strict constraint on the sample selection from a large photometric database, if one desires to obtain an unbiased sample against metallicity. Unfortunately, there is no adequate distance–mass bin that is essentially bias-free over a large range in metallicity. Instead, we focused our analysis on metal-poor stars ([Fe/H] < -1.2) to construct an unbiased MDF of the halo system, as in A13.

Photometric metallicities are sensitive to the size of photometric errors in the *u* passband, because the technique

Table 1
Photometric Metallicity Distribution Function from Stripe 82

[Fe/H]	$N_{\rm stars}$	$N_{\rm stars}$ (Corr)[a]
−1.05	257	245
−1.15	316	313
−1.25	407	364
−1.35	420	461
−1.45	499	487
−1.55	405	393
−1.65	366	392
−1.75	371	398
−1.85	413	410
−1.95	322	362
−2.05	224	231
−2.15	185	196
−2.25	181	179
−2.35	154	179
−2.45	148	149
−2.55	98	114
−2.65	71	94
−2.75	68	57
−2.85	29	26
−2.95	37	41

Notes. Our sample selection is biased against stars with [Fe/H] > -1.2 (see A13).
[a] After applying photometric zero-point corrections in Yuan et al. (2015b).

relies on strong metallic-line blanketing in this short wavelength band. In A13, we used photometry of stars with $\sigma_u < 0.03$ mag, or $u < 20.6$ mag and $u < 21.0$ mag in the calibration (Ivezić et al. 2007) and co-added (Annis et al. 2014) catalogs, corresponding to maximum heliocentric distances of ∼7.8 kpc and ∼9.4 kpc, respectively. With the new co-add catalog of J14, we can extend our photometric metallicity estimates of stars out to ∼10.5 kpc from the Sun, by virtue of its fainter u-band limit ($\sigma_u = 0.03$ mag at $u = 21.3$ mag).

Other sample-selection criteria are the same as in A13: stars must be detected in all five *ugriz* pass bands, with a reduced χ^2 value of a model fit less than 3 for each star, and located at high Galactic latitudes ($|b| > 35°$), with a minimum heliocentric distance of 5 kpc in order to minimize contamination from disk-system stars. A minimum mass of 0.65 $M_\odot$ was set by the minimum heliocentric distance and the above mass–luminosity–metallicity limit. The maximum stellar mass was set to 0.75 $M_\odot$, since stars with $M_* \sim 0.75\ M_\odot$ are near the main-sequence turn-off at the lower end of our metallicity estimate ([Fe/H] $= -3$).

4. UPDATED HALO MDFS AND METALLICITY–KINEMATICS CORRELATIONS

Our updated MDF of the halo is presented as a black histogram in Figure 1 (see also Table 1), which comprises a stellar sample that is almost a factor of two larger ($N = 4971$ at [Fe/H] < -1) than those of the Ivezić et al. (2007, red histogram; $N = 2484$) or the Annis et al. (2014, blue histogram; $N = 2457$) catalogs used in our previous effort. All three SDSS catalogs are enormously larger than the kinematically selected stars in the solar neighborhood from Ryan & Norris (1991), for which the MDF is shown in the gray shaded region. The black dotted histogram in the top panel shows the same MDF as the black solid histogram, but after applying photometric zero-point corrections as proposed by Yuan et al. (2015b) in both the scan and camcol directions; the differences are negligible. The bottom panel of Figure 1 shows cumulative distributions of these MDFs; the shape of our new MDF is similar to those from the previous samples.

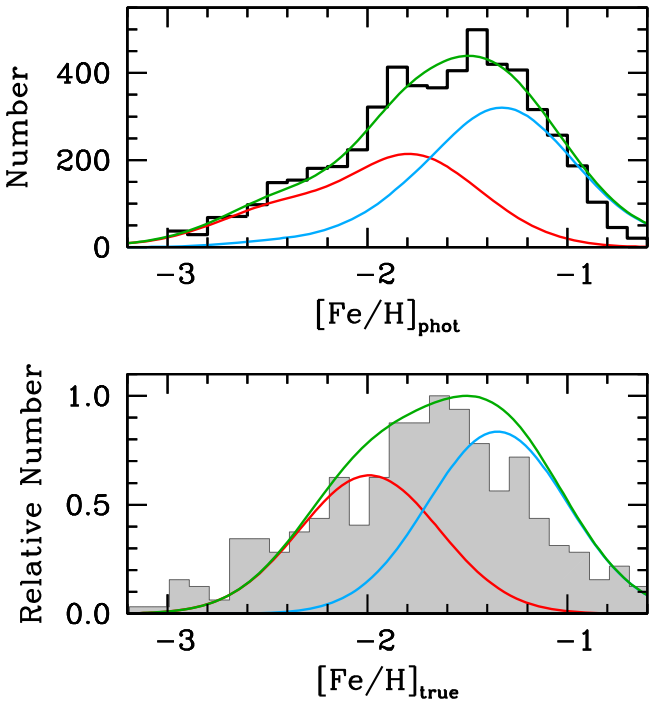

Figure 2. Top panel: the observed photometric MDF of the new co-added sample (black histogram), and its deconvolution using two components (red and blue lines). Each curve represents a MDF with a Gaussian metallicity distribution (shown in the bottom panel), convolved with error+binary models as described in A13. The green curve is a sum of these two components. Bottom panel: the modeled input components (red and blues lines, with dispersions of 0.4 dex, respectively) and the resulting mixture (green line). The MDF in the solar neighborhood from Ryan & Norris (1991) is shown as a gray histogram for comparison.

Figure 2 is a decomposition of the newly determined MDF, under the assumption that the diffuse halo system is composed of two spatially overlapping populations of stars. Specifically, we adopted the working hypothesis that these MDFs can be described as Gaussian distributions in [Fe/H], with a dispersion of $\sigma = 0.4$ dex for each component. As in A13, we did not employ the simple mass-loss modified model in a leaky box (e.g., Hartwick 1976), since such models are based on unphysical (and unproven) assumptions on the instantaneous recycling and mixing of metals, which are incompatible with a presumed hierarchical assembly of the Galactic halo from individual lower-mass subhalos. The red and blue lines in the top panel show the division of the observed MDF, which take into account the smearing due to photometric errors and unresolved binaries in the sample. The green line is a sum of these two MDFs. The peak of the (deconvolved) metal-rich component is [Fe/H] $= -1.38 \pm 0.26$, while that of the metal-poor component is [Fe/H] $= -1.94 \pm 0.29$, with little dependence on the choice of the dispersion in [Fe/H]. Our estimated metallicity peaks are systematically ∼0.2 dex higher than the (spectroscopic) values ([Fe/H] $= -1.6$ and -2.2, respectively) found by Carollo et al. (2007).

About 10% of the stars in our sample are found at [Fe/H] < -2.3, as is also the case for the Ryan & Norris sample. The estimated fraction of the metal-poor component amounts to

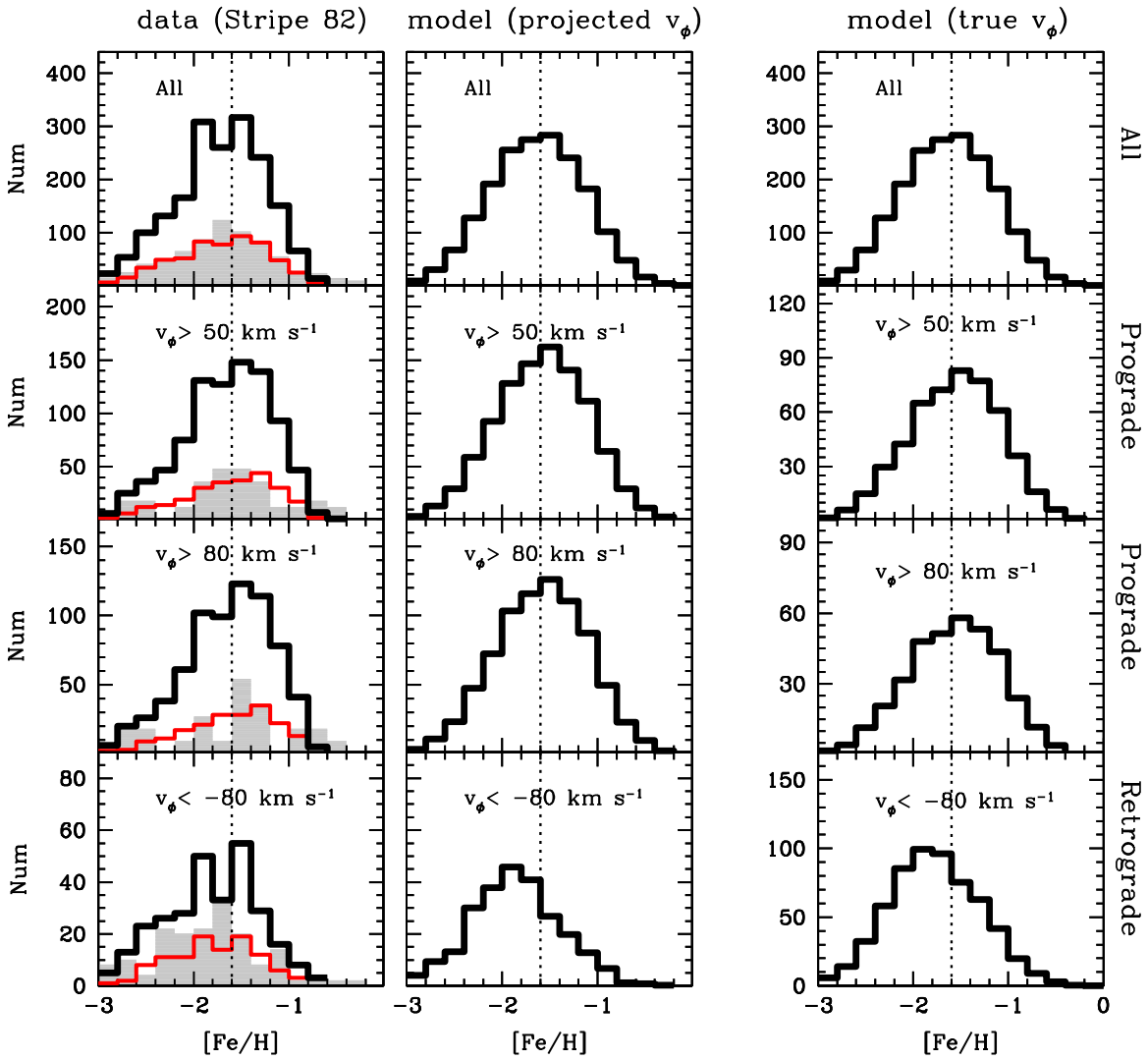

Figure 3. Left column: changes in the observed MDF of local halo-system stars for different cuts in v_ϕ. The black histogram shows MDFs of stars at $|b| > 45°$, and the red histogram shows those with $|b| > 60°$. The gray histograms display local MDFs from Ryan & Norris (1991), after multiplying their MDF by an arbitrary factor to approximately match the histograms of the high-latitude sample. There is a clear preference for low-metallicity stars to be found in greater number, relative to metal-rich stars, in the retrograde cuts compared to the prograde cuts. Middle column: halo MDFs as derived from the best-matching Milky Way models, assuming a fractional contribution of 55% from inner-halo stars in our sample volume. The same sample cuts in v_ϕ (and $|b| > 45°$) are shown as in the left column, but v_ϕ is derived from proper motions in the mock catalog. Right column: same as in the middle panels, but based on v_ϕ derived from full kinematic information in the mock catalog.

∼40%–45%, depending on the assumed size of a dispersion in [Fe/H] for each component ($\sigma \sim 0.2$–0.4 dex). When the peak metallicity of the inner-halo component changes by ±0.1 dex, the peak metallicity of the outer-halo component also changes by approximately 0.1 dex (positively correlated). The fraction of inner/outer halo increases/decreases by ∼15% when the peak metallicities decreases by 0.1 dex. Interestingly, the fractional contribution from the metal-poor component is larger than that found in A13 (∼30%), perhaps because we included more distant stars in our sample from the J14 catalog.

In order to inspect the properties of the two chemically and kinematically distinct populations, we combined our photometric metallicity estimates with approximate Galactocentric rotational velocities (v_ϕ). While a v_ϕ determination requires full kinematic information from both radial-velocity and proper-motion measurements, proper motions alone (combined with distances) can be used to derive approximate rotational velocities for stars at high Galactic latitudes. The left-hand column in Figure 3 shows MDFs from our new co-add sample. The black histograms are MDFs of stars at $|b| > 45°$, with good proper-motion measurements from Munn et al. (2004). The red histograms are stars with $|b| > 60°$, which should yield more accurate estimates of v_ϕ. For comparison, the gray shaded histogram represents the MDF from Ryan & Norris (1991) based on full space motions.

In the lower rows of panels shown in Figure 3, we divided our sample stars based on their rotational velocities, either prograde ($v_\phi > 50\,\mathrm{km\,s^{-1}}$ or $v_\phi > 80\,\mathrm{km\,s^{-1}}$)[5] or retrograde ($v_\phi < -80\,\mathrm{km\,s^{-1}}$). As can be seen from comparison of the lower two panels in the left-hand column, there is a clear shift in the MDFs for stars in the prograde and retrograde subsamples. The median metallicity of stars ($|b| > 45°$) with prograde rotations (third panel) is [Fe/H] = −1.6, while that of stars with retrograde rotations (bottom panel) is [Fe/H] = −1.8.

[5] The $v_\phi > 50\,\mathrm{km\,s^{-1}}$ cut in the second row of panels was added due to the small number of stars in the Ryan & Norris (1991) sample with $v_\phi > 80\,\mathrm{km\,s^{-1}}$.

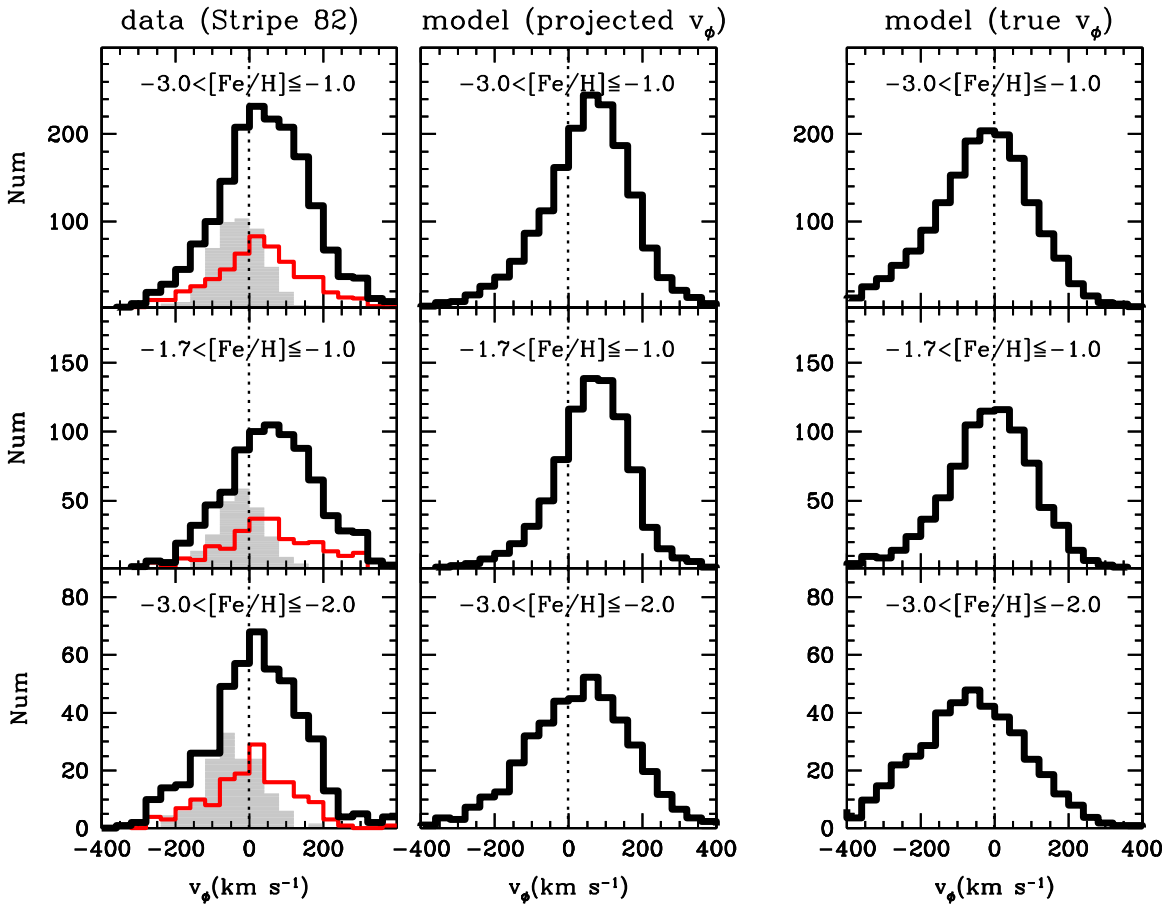

Figure 4. Same as in Figure 3, but showing the v_ϕ distribution for different sample cuts in metallicity.

A Kolmogorov–Smirnov (K–S) test rejects a null hypothesis that the two distributions were drawn from the same underlying population at high levels of significance ($p = 0.00004$ for $|b| \geqslant 45°$; $p = 0.007$ for $|b| \geqslant 60°$). These results are even more statistically significant than found by A13 for the Annis et al. (2014) co-add catalog, due to the factor of two increase in the number of stars included in the halo sample, suggesting that the Milky Way halo system comprises at least two stellar populations with distinct metallicity–kinematics properties (e.g., Carollo et al. 2007, 2010; Beers et al. 2012). Note that similar differences are seen for the Ryan & Norris (1991) solar-neighborhood sample (which has been rescaled to match the numbers found for our present high-latitude sample).

Similarly, the left-hand column in Figure 4 shows the distribution of v_ϕ for stars in Stripe 82. The top panel in this column contains our sample stars with photometric metallicities $-3 < [\mathrm{Fe/H}] \leqslant -1$. Stars in the middle panel are stars with higher metallicities ($-1.7 < [\mathrm{Fe/H}] \leqslant -1$) than those shown in the bottom panel ($-3 < [\mathrm{Fe/H}] \leqslant -2$). Comparison between the lower two panels clearly shows that high-metallicity halo stars are, on average, rotating faster in the same direction as the disk ($\langle v_\phi \rangle = +61 \pm 5\,\mathrm{km\,s^{-1}}$, while those with lower metallicities are rotating more slowly ($\langle v_\phi \rangle = +16 \pm 6\,\mathrm{km\,s^{-1}}$). A K–S test rejects a null hypothesis that the two distributions were drawn from the same underlying population at high levels of significance ($p = 10^{-6}$ for $|b| \geqslant 45°$; $p = 0.006$ for $|b| \geqslant 60°$).

To provide a check on our inferences, we examine the behavior of simulated samples of main-sequence stars selected from mock catalogs created by running `galfast` (Jurić et al. 2008; Juric et al. 2010). We considered chemically and kinematically distinct stellar components in the halo with fixed ratios of contributions, ranging from 10% to 90% of inner-halo stars (90%–10% outer-halo stars), with a 10% increment. Instead of deriving photometric metallicities of stars from synthetic color–magnitude diagrams in the mock catalog, we directly assigned stellar metallicities by drawing from parent Gaussian metallicity distributions with peaks at $[\mathrm{Fe/H}] = -1.38$ and -1.94 for the inner and outer halos, respectively, each of which has a metallicity dispersion of $\sigma = 0.4$ dex. We adopted the parameters of the velocity ellipsoids (and derived power-law slopes) in the halo system from Carollo et al. (2010), where the mean rotational velocities of the two components are $\langle v_\phi \rangle = +7\,\mathrm{km\,s^{-1}}$ and $-80\,\mathrm{km\,s^{-1}}$, respectively (when $v_{\phi,\mathrm{LSR}} = +220\,\mathrm{km\,s^{-1}}$), and power-law slopes of -3.17 and -1.79 for the inner- and outer-halo density profiles, respectively. We generated mock catalogs of stars along the Stripe 82 footprint with the same limit in Galactic latitude ($|b| > 45°$). To match our mass–luminosity–metallicity criterion, we restricted simulated stars to $4 \leqslant M_r \leqslant 6$ (see Figure 11 in A13), along with $5 \leqslant d_{\mathrm{Sun}} \leqslant 10$ kpc.

The middle and right-hand columns in Figures 3 and 4 show the predicted MDFs and v_ϕ distributions from `galfast`, when the modeled contribution from the inner halo is set to 55% in our sample volume. Each panel shows a distribution of stars with the same v_ϕ (or [Fe/H]) cut as in the left-hand column. In the middle column, we used a "projected v_ϕ," computed from proper motions and distances as in our observed data set. Since our

Stripe 82 sample extends over $60^\circ \lesssim l \lesssim 180^\circ$ and $-65^\circ \lesssim b \lesssim -45^\circ$, these projected v_ϕ values are systematically higher than the true rotation velocities based on full kinematic information from the mock catalog (right-hand column).

As shown in the lower panels in the middle column of Figure 3, a shift in the peak metallicity (and tails) of the simulated data set is clearly present, similar in nature to the observed data set, when divided into stars with prograde and retrograde orbits. Each subsample includes both inner- and outer-halo stars, because of their large velocity dispersions, but the shift in the overall MDFs can be understood as due to the different contributions from each of the components in the v_ϕ cuts. We looked for the best-matching fraction of inner/outer halos in the models by changing their relative contributions, and found that ∼45%–65% inner-halo fractions provide acceptable matches to the observed MDFs and v_ϕ distributions in Figures 3 and 4. Lower (or higher) inner-halo fractions result in a significant enhancement (or depression) of the outer-halo component, yielding incompatible matches to these distributions. In all cases, a single-population diffuse-halo model is rejected.

5. CONCLUSIONS

In this letter we have employed the deep photometric co-add catalog of Stripe 82 (J14) to derive new estimates of photometric metallicities for halo main-sequence stars, and obtained a fair MDF based on more distant in situ samples of stars than available in our previous work. Our results show that stars with retrograde orbits have, on average, lower metallicities than stars with prograde rotations, consistent with previous results from A13, but with even higher statistical significance. The estimated fraction of the metal-poor or outer-halo component in the local volume is $\sim 45\% \pm 10\%$.

The presence of two distinct diffuse stellar halos implies that the formation of the halo system must have involved at least two different star formation episodes. According to recent theoretical models (e.g., Johnston et al. 2008; Zolotov et al. 2009; McCarthy et al. 2012; Tissera et al. 2012, 2013), inner-halo population stars formed from more massive sub-halos, or dwarf galaxies with sufficient gas content that could reach the inner region of the proto-Galaxy through dynamical friction, or formed in situ in the inner region from the rapid collapse of primordial gas. Sustained star formation in this region would lead to higher metallicity. In contrast, stars of the outer-halo population formed in lower mass dwarf galaxies, and were brought into the main halo of the Milky Way through disruption and accretion, resulting in a diffuse outer halo with distinct and significantly hotter kinematics, which is present throughout the halo system of the Galaxy, including the inner-halo region. A limited star formation history, perhaps involving no more than a single burst, would lead to lower metallicity. The situation is likely to be complex, and dependent on both the star formation history within individual sub-halos, and on their merger and accretion histories (see discussions by Johnston et al. 2008 and Tissera et al. 2013). In any event, one would expect to find samples of old stars arising from both populations in the local volume. This interpretation has received recent support from the identification by Santucci (2015) of the so-called "ancient chronographic sphere," a region comprising the oldest stars in the Milky Way located within 15 kpc from the Galactic center, and extending into the region we have analyzed in the present paper.

Our work is limited by the photometric precision and kinematic measurement errors in the currently available survey data, as well as the relatively small volume of space explored by Stripe 82. However, it clearly demonstrates the feasibility of dissecting stellar populations in more distant regions of the halo with future large photometric and astrometric surveys such as the Large Synoptic Sky Survey (Ivezic et al. 2008b) and *Gaia* (Perryman et al. 2001).

We thank Mario Jurić for his help with `galfast`. D.A. and Y.S.L. acknowledge support provided by the National Research Foundation of Korea to the Center for Galaxy Evolution Research (No. 2010-0027910). D.A. was partially supported by Basic Science Research Program through the National Research Foundation of Korea (NRF) funded by the Ministry of Education (2010-0025122). T.C.B., V.M.P., and D.C. acknowledge partial support for this work from grant PHY 14-30152; Physics Frontier Center/JINA Center for the Evolution of the Elements (JINA-CEE), awarded by the US National Science Foundation. R.M.S. and S.R. would like to thank partial support from FAPESP, CNPq, and CAPES. Y.S.L. acknowledges partial support from the Basic Science Research Program through the National Research Foundation of Korea (NRF) funded by the Ministry of Science, ICT & Future Planning (NRF-2015R1C1A1A02036658).

REFERENCES

Allende Prieto, C., Fernandez-Alvar, E., Schlesinger, K. J., et al. 2014, A&A, 568, 7
An, D., Beers, T. C., Johnson, J. A., et al. 2013, ApJ, 763, 65 (A13)
Annis, J., Soares-Santos, M., Strauss, M. A., et al. 2014, ApJ, 794, 120
Beers, T. C., Carollo, D., Ivezić, Ž., et al. 2012, ApJ, 746, 34
Beers, T. C., & Christlieb, N. 2005, ARA&A, 43, 531
Carollo, D., Beers, T. C., Bovy, J., et al. 2012, ApJ, 744, 195
Carollo, D., Beers, T. C., Chiba, M., et al. 2010, ApJ, 712, 692
Carollo, D., Beers, T. C., Lee, Y. S., et al. 2007, Natur, 450, 1020
Carollo, D., Freeman, K., Beers, T. C., et al. 2014, ApJ, 788, 180
Chen, Y. Q., Zhao, G., Carrell, K., et al. 2014, ApJ, 795, 52
de Jong, J. T. A., Yanny, B., Rix, H.-W., et al. 2010, ApJ, 714, 663
Fernandez-Alvar, E., Allende Prieto, C., Schlesinger, K. J., et al. 2015, A&A, 577, 81
Font, A. S., McCarthy, I. G., Crain, R. A., et al. 2011, MNRAS, 416, 2802
Frebel, A., & Norris, J. E. 2015, ARA&A, 53, 631
Hartwick, F. D. A. 1976, ApJ, 209, 418
Ivezić, Ž., Sesar, B., Jurić, M., et al. 2008a, ApJ, 684, 287
Ivezić, Ž., Smith, J. A., Miknaitis, G., et al. 2007, AJ, 134, 973
Ivezic, Z., Tyson, J. A., Abel, B., et al. 2008b, arXiv:0805.2366
Janesh, W., Morrison, H. L., Ma, Z., et al. 2015, ApJ, submitted (arXiv:1503.09133)
Jiang, L., Fan, X., Bian, F., et al. 2014, ApJS, 213, 12 (J14)
Johnston, K. V., Bullock, J. S., Sharma, S., et al. 2008, ApJ, 689, 936
Juric, M., Cosic, K., Vinkovic, D., & Ivezic, Z. 2010, BAAS, 42, 401.25
Jurić, M., Ivezić, Ž., Brooks, A., et al. 2008, ApJ, 673, 864
McCarthy, I. G., Font, A. S., Crain, R. A., et al. 2012, MNRAS, 420, 2245
Munn, J. A., Monet, D. G., Levine, S. E., et al. 2004, AJ, 127, 3034
Nissen, P. E., & Schuster, W. J. 2010, A&A, 511, L10
Norris, J. E., & Ryan, S. G. 1991, ApJ, 380, 403
Perryman, M. A. C., de Boer, K. S., Gilmore, G., et al. 2001, A&A, 369, 339
Ryan, S. G., & Norris, J. E. 1991, AJ, 101, 1865
Santucci, R. M., Beers, T. C., Placco, V. M., et al. 2015, ApJL, 813, L16
Schönrich, R., Asplund, M., & Casagrande, L. 2011, MNRAS, 415, 3807
Schuster, W. J., Moreno, E., Nissen, P. E., & Pichardo, B. 2012, A&A, 538, A21
Tissera, P. B., Scannapieco, C., Beers, T. C., & Carollo, D. 2013, MNRAS, 432, 3391
Tissera, P. B., White, S. D. M., & Scannapieco, C. 2012, MNRAS, 420, 255
Yuan, H., Liu, X., Xiang, M., Huang, Y., & Chen, B. 2015a, ApJ, 803, 13
Yuan, H., Liu, X., Xiang, M., et al. 2015b, ApJ, 799, 133
Zolotov, A., Willman, B., Brooks, A. M., et al. 2009, ApJ, 702, 1058